The Evolving Metropolis
2019 IABSE Congress New York City

IABSE 90 YEARS

The structural behavior of tiled laminate GFRP composites, a class of robust materials for civil applications

Wouter DE CORTE
Professor
Ghent University
Ghent - Belgium
wouter.decorte@ugent.be

WDC is associate professor in the field of numerical and experimental analysis of civil structures.

Jordi UYTTERSPROT
Ing
Ghent University
Ghent - Belgium
jordi.uyttersprot@ugent.be

JU is PhD student working on structural behaviour of tiled laminate composites for civil applications.

Wim VAN PAEPEGEM
Professor
Ghent University
Ghent - Belgium
wim.vanpaepegem@ugent.be

WVP is full professor in the field of experimental and computational mechanics of fibre-reinforced composite materials for engineering applications.

Contact: wouter.decorte@ugent.be

1 Abstract

This paper focuses on the structural behavior of tiled laminate composites. Such laminates, in which the plies are not parallel to the outer surfaces are found in GFRP bridge deck panels. The technology is developed for the construction of robust GFRP panels useful in highly loaded structures such as bridges or lock gates. In civil structures, the drawback in traditional FRP sandwich structures has always been debonding of skin and core. Such a debonding problem may occur after unintentional impact, followed by fatigue loading. Through the concept of using overlapping Z-shaped and two-flanged web laminates, alternating with polyurethane foam cores, debonding is no longer possible in vacuum infused GFRP bridge deck panels. In such panels, the fibers in the upper and lower skins as well as in the vertical webs run in all directions, rendering a resin-dominated crack propagation impossible. As a result of the integration of core and skin reinforcement, a skin material is created in which the reinforcement is not parallel to the outer surfaces, but tiled. Based on experimental results and numerical simulations the relevance of tiled laminates for civil applications is demonstrated.

Keywords: tiled laminate, tiled sandwich, composite, GFRP, finite element analysis, Abaqus, failure behavior

2 Introduction

The tiled laminate panel technology is developed for the construction of a robust glass fiber reinforced polymer (GFRP) panel applicable for highly loaded structures [1-4]. The inherit drawback of traditional FRP sandwich structures in civil engineering has always been debonding of skin and core) due to impact followed by fatigue loading. Using the tiled laminate concept, such skin-core debonding is no longer possible. Figure 1 shows an exploded view of an tiled laminate sandwich panel. The panel consists of multiple foam cores over which single fiber mats and Z-shaped fiber mats are draped according to a predefined configuration. The panel's span direction corresponds to the longitudinal direction of the core elements.

Figure 1. Exploded view of an tiled laminate sandwich bridge deck panel

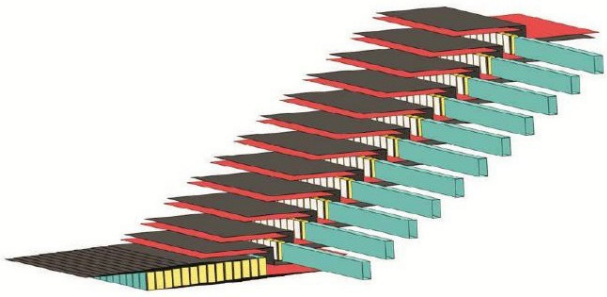

Each fiber layer is thus part of the top skin of the panel, the core and the bottom skin of the panel. Due to this full integration of skins and core, skin-

core debonding is essentially not an option. This enables the use of the panels as bridge deck or lock gate panels. Additionally, and as a result of this specific sandwich configuration, the fiber plies within the skins are positioned at a slight angle with respect to the horizontal finishing surface.

A laminate is thus obtained with laminae (plies) that have a small but distinct out-of-plane angle. Because the knowledge of such out-of-plane layered composite materials is still rather limited, the behavior of these types of laminates cannot be interpreted correctly. Consequently, they require a larger safety factor in practical applications. To achieve more insight into the material behavior, especially concerning the stiffness, the interlaminar shear strength and the ultimate strength, numerical as well as experimental research of these *tiled laminate composites* is required.

3 Numerical analysis of a tiled laminate

In what follows, the results of a nonlinear finite element analysis of a tiled laminate are shown. This includes a discussion of the numerical model, the tensile behavior in the tiled direction, the interlaminar behavior and the flexural behavior.

3.1 Numerical model

A tiled laminate specimen, with material properties and dimensions typical for the top skin of a tiled sandwich panel is simulated in Abaqus [5]. Modelling is done at the mesoscale level, meaning that the laminate is represented by a stacking of composite plies (fiber fabric surrounded by resin) and interfaces (resin layers), rather than modelling individual fibers at microscale level. Interlaminar failure is possible in the cohesive interface elements between the plies, while intralaminar failure is based on the Hashin criterion for each ply. Delamination of the fibers within one composite ply is considered as fabric and resin are modelled together. The specimen consists of three repetitive fabric stackings, each composed of 4 individual plies. In the direction of the specimen each stacking contains two 90◦-plies, one -45◦-ply and one +45◦-ply. A total of 12 composite plies and 11 interfaces is thus obtained. It might be surprising to the reader that there are no 0° fabrics present in the specimen. However, the main load carrying direction in civil structures (e.g. bridge decks) is typically perpendicular to the tiling direction, explaining the absence of 0° fabrics here.

As the composite plies are modelled with a thickness of 0.87mm and the interfaces with a thickness of 0.05mm (50µm), the total specimen thickness equals 10.99mm. This is a common value for skins of composite panels in civil engineering structures. The geometry of the specimen is shown in Figure 2. Note that only the 4-ply stackings are visualized in the figure (not the individual plies). Every 100 mm one ply stacking package is added to the bottom side and one package is removed from the top side. This corresponds to a core width of 100mm and a three-way overlap (Figure 1). As a consequence a ply inclination of 2,11° is generated. The total specimen length is taken equal to 500mm and the width equal to 20 mm. Boundary and loading conditions depend on the mechanical test that is simulated and will thus be mentioned in the following paragraphs.

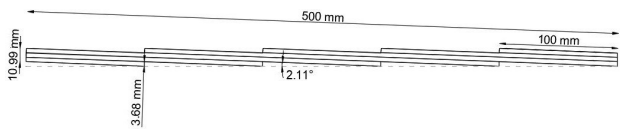

Figure 2. Geometry of the numerical model

The materials defined in the numerical model are based on the material properties as mentioned in manufacturer's documentation [6]. With respect to the interfaces, cohesive elements (COH3D8) with traction-separation response are used for the interfaces. Table 1 shows the material properties of the resin corresponding to an interface thickness of 50 µm. Homogeneous continuum shells (SC8R) make up the composite plies consisting of E-glass fibers embedded in a polyester resin. The combined material properties are defined using the ElamX^2 software [7], based on the known material properties of the resin and the fibers [6], the ply thickness of 0.87 mm and the fiber content within the ply (56%). The resulting ply moduli are shown in Table 2.For the failure/damage, the Hashin criterion is chosen. Table 2 gives an overview of the damage parameters. In this, the subscripts 't' and 'c' represent respectively tension and compression, while the symbols // and ⊥ indicate the direction respectively along and perpendicular to the fiber direction.

Table 1. Interfacial properties

Moduli	E/E_{nn}	74000	MPa
	G_1/E_{ss}	28000	MPa
	G_2/E_{tt}	28000	MPa
Failure stress	σ_n	90	MPa
	σ_1	90	MPa
	σ_2	90	MPa
Fracture energy	G_{fn}	60	J/m²
	G_{f1}	150	J/m²
	G_{f2}	150	J/m²
Density	ρ	1.09E-9	ton/mm³

Table 2. Composite ply properties

Moduli	E_1	42488	MPa
	E_2	7970	MPa
	E_3	3700	MPa
	G_{12}	2973	MPa
	G_{13}	1400	MPa
	G_{23}	1400	MPa
	ν_{12}	0.05	-
	ν_{13}	0.265	-
	ν_{23}	0.265	-
Hashin damage initiation	$\sigma_{t//}$	840	MPa
	$\sigma_{c//}$	630	MPa
	$\sigma_{t\perp}$	44	MPa
	$\sigma_{c\perp}$	160	MPa
	$\tau_{max//}$	45	MPa
	$\tau_{max\perp}$	45	MPa
Damage evolution	$G_{t//}$	8300	J/m²
	$G_{c//}$	4700	J/m²
	$G_{t\perp}$	100	J/m²
	$G_{c\perp}$	1600	J/m

3.2 Numerical tensile test

To simulate a displacement controlled tensile test, the right face of the specimen (Figure 2) is given a displacement while the left face of the specimen remains stationary.

3.2.1 Elastic properties (Abaqus/Standard)

First, an equivalent homogenized longitudinal stiffness modulus is determined. Figure 3 shows the equivalent stiffness of the model in function of average longitudinal strain. The basic model (50µm interface) renders an equivalent stiffness of 8642 MPa without considering geometric non-linearity (NLGEOM OFF). If this non-linearity is considered the equivalent stiffness increases slightly with the strain indicating a minute straightening effect.

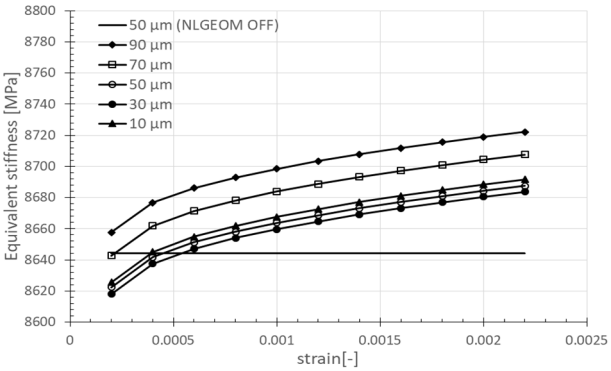

Figure 3. Equivalent longitudinal stiffness (interfacial thickness variation)

Additionally the influence of the thickness of the interface layers on the longitudinal stiffness is investigated. For this five different interface thicknesses are considered (See Figure 3). However, when increasing the interface thickness, also the total laminate thickness will increase which is undesirable. Therefore, the ply thicknesses as well as the ply moduli, considering the resulting change in fiber content, are adjusted. Figure 3 indicates a difference less than 1%. Should the moduli not have been adjusted, the difference would be close to 10%.

Also the influence of the out-of-plane angle on this equivalent stiffness is investigated (See Figure 4). For this, the specimen length, width, thickness and overlap configuration are maintained while the stacking angle is changed. To achieve this the core width is modified accordingly.

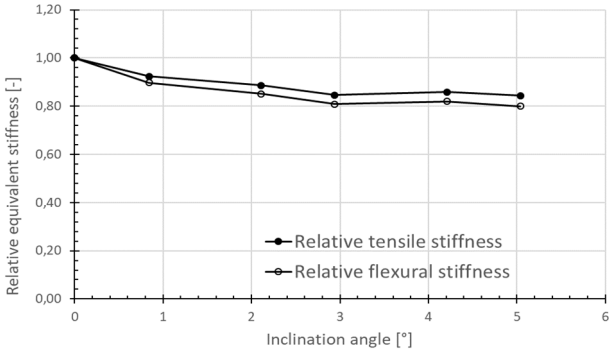

Figure 4. Relative equivalent longitudinal and flexural stiffness (angle variation)

With respect to the stiffness of the plane-parallel specimen (0°) a 10 to 15 percent decrease in longitudinal stiffness is observed. Given the

robustness and production advantages [1-2], this is acceptable.

3.2.2 Tensile failure (Abaqus/Explicit)

To predict laminate strength, the progressive accumulation of damage leading to ultimate failure needs to be taken into account in the calculations. This can be done by creating Abaqus/Explicit models. To achieve low accelerations and to eliminate dynamics as much as possible, a mass scaling factor of 100 is chosen.

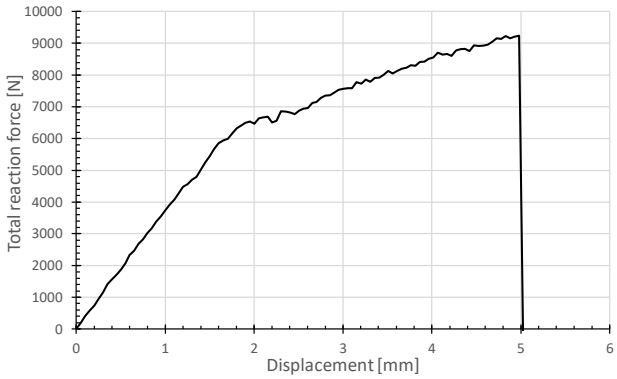

Figure 5. Force-displacement diagram (basic model)

Figure 5 shows the force-displacement diagram, while figure 6 shows the deformed shape near ultimate failure of the basic 2°-model. The reaction force reaches a maximal value of 9239N at a 5mm displacement. This is equivalent to a laminate tensile failure strength of 42 MPa at an equivalent strain of 1%.

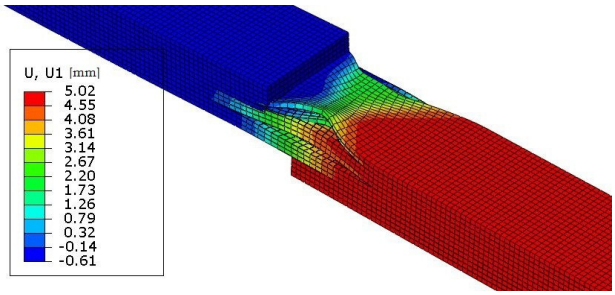

Figure 6. Deformed shape at ultimate failure (basic model – exaggerated)

The location of ultimate failure is situated at a reduced cross section of the specimen, where only 8 plies are present instead of 12. The first sign of failure occurs at a displacement of 1.05 mm, when the Hashin matrix tensile damage criterion (HSNMTCRT) reaches its total capacity. At this moment, the interface (SDEG) criterion reaches only 28% (24.73 MPa) of its maximum stress of 90 MPa. The first interlaminar failure occurs at a displacement of 2.7 mm only indicating that the stacked configuration does not lead to premature interlaminar failure.

To investigate the influence of the interfacial failure properties on the laminate strength, the nominal stresses of the normal mode (I) and shear modes (II and III) are varied.

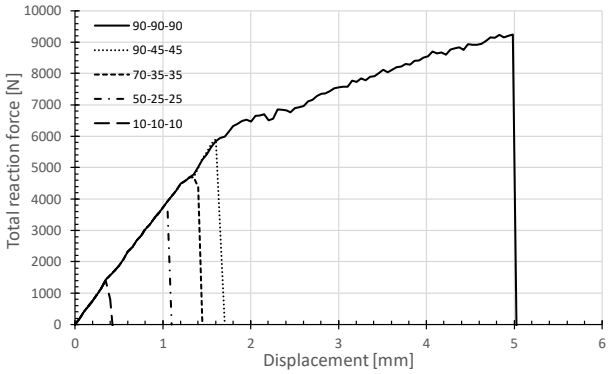

Figure 7. Force-displacement diagram (interfacial strength variation)

Based on the resulting force-displacement diagrams of Figure 7 it is clear that the shear mode interfacial strength is the most influential on the specimen's tensile strength, while the normal mode strength is of minor importance. Lowering the interfacial properties also has an influence on the failure initiation. In Figure 8 (10-10-10), the specimen fails due to delamination between the fiber stackings, in contrast to the intralaminar failure of Figure 6.

Figure 8. Deformed shape at ultimate failure (low interfacial strength)

Also the influence of the out-of-plane angle on the laminate strength is investigated. Figure 9 shows the relative strength of the numerical specimens with respect to the strength of a plane-parallel specimen. The shape of the diagram shows large similarities to the diagram in Figure 4. It is clear that the plane-parallel specimen is roughly 20% stronger than the other specimens, but the additional influence of the angle is limited. This can be attributed to a combination of a smaller effective

section in the failure zone, stress concentrations due to the local geometry of the numerical specimen, and an eccentricity between the resultant tensile force and the local section, introducing local second order bending. Although this reduction is larger than for the equivalent stiffness, it is acceptable in view of the aforementioned advantages [1-2].

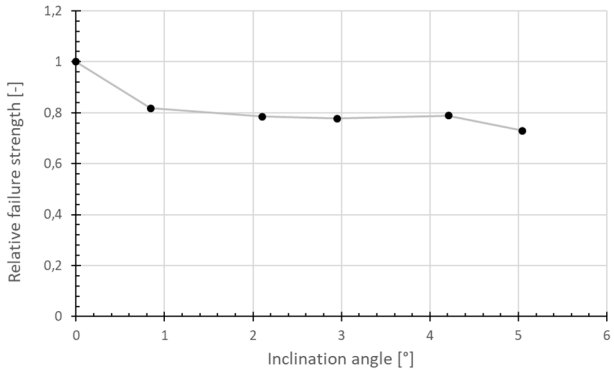

Figure 9. Relative tensile strength (angle variation)

3.3 Numerical shear test

Next to the tensile strength of the laminate, also the interlaminar shear strength is of importance. In order to assess the numerical model, the results are compared to a preliminary physical shear test. The specimen dimensions are L=172mm, W=32.5mm, T=10.99mm, span=150mm. The fiber stacking of the tested specimen is [0/0/+45/-45], in order to fulfil the requirement of ASTM Standard D2344 to have at least 10% of the fibers parallel to the span direction [7] to avoid premature failure due to bending. The specimen is thus taken perpendicular to the stacking direction. The test set-up consists of two cylindrical supports spaced at … mm and a loading nose. To achieve good results, a maximum load rate of 5mm/s and a soft start had to be imposed together with a linear elastic zone (L=100mm, T=4 plies) underneath the loading nose. The numerically obtained force-displacement graph is quite close to the practical results (See figure 10), not only with respect to the bending and shear stiffness (slope of the first branch of the diagram), but also with respect to the interlaminar shear strength (18.77 MPa numerically, 18.97 MPa experimentally. It should be noted that in order to determine the ILSS correctly, the failure mode should represent interlaminar shear failure. This is not the case for the numerical model as it is the matrix in the bottom composite plies that fails in tension (HSNMTCRT) due to the strong bending conditions.

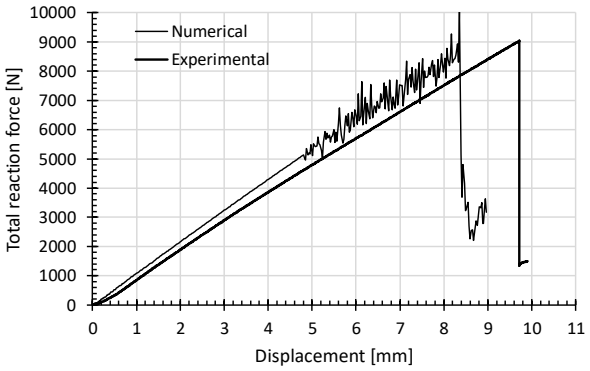

Figure 10. Force-displacement diagram (shear test)

To examine the failure behavior more in detail, a short beam shear test set-up is simulated according to the specifications of ASTM Standard D2344 [7]. The ASTM Standard prescribes the specimen dimensions with respect to the specimen thickness, in this case L=65.94 mm, W=21.98 mm, T=10,99mm, span=43.96mm. Again the modified fiber stacking [0/0/+45/-45] is used, and to avoid premature failure due to load introduction, linear zones are introduced underneath the loading nose and above the supports. Figure 11 shows the deformed shape of the numerical specimen at ultimate failure. One can clearly see that delamination occurs between the 45°-plies. The ILSS of this numerical specimen is determined to be 59 MPa.

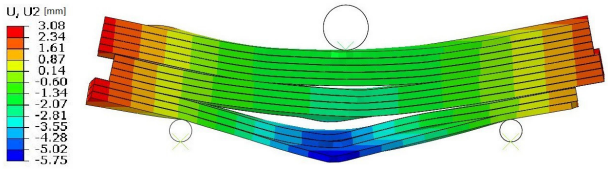

Figure 11. numerical ILSS test

A similar failure behavior is obtained when the interfacial shear strength is lowered from 90 MPa (Table I) to 45 MPa. The ILSS then becomes equal to 33 MPa.

Table 3 gives values for the short beam strength from samples taken from the top and bottom skin from a tiled sandwich bridge deck. The values indicate that in practice the interfacial strength to be used in the finite element models is in between the 45 and 90 MPa and also depends on the

compaction during infusion since upper and lower skin values are about 10% different. Further study will provide more detailed values.

Table 3. Measured ILSS values (SBS) [MPa]

	Upper skin	Lower skin	Average
Mean	33.84	36.65	35.25
Std. Dev.	5.37	3.47	4.58
CV	15.87	9.47	13.00

3.4 Numerical flexural test

Finally, a numerical displacement controlled three-point bending test is performed based on the test specimen of Figure 2. Figure 4 gives the relative flexural stiffness of each specimen with respect to the plane-parallel specimen. The decrease in stiffness for an increasing out-of-plane angle is somewhat higher than in case of a tensile test at about 15 to 20%. The explanation of paragraph 3.2 still stand, being somewhat more pronounced in this case.

4 Conclusions

Although the concept of tiled sandwiches and tiled laminates, and it's robustness have been demonstrated, little is known about the way to model these at the meso level. This paper presents a way to numerically model such concepts at the meso level combining continuum shell elements with a Hashin failure criterion and cohesive elements with a traction separation law. The results indicate a 10 to 15% reduction of longitudinal stiffness, a 15 to 20% reduction of flexural stiffness and a 20% reduction of tensile strength. It is shown that for the given configuration, intralaminar damage initiates failure, while the interlaminar failure occurs at a later stage. Evidently, more numerical and experimental analyses are required to fully understand the mechanical behavior of this promising concept for FRP based robust civil structures.

5 Acknowledgements

The authors wish to acknowledge Frede Ten Vergert, Liza Leeman, Dries Desmijter, Lorin Peeters for their respective contributions in the numerical modelling and the experiments, and to thank Fibercore Europe for the bridge deck samples.

6 References

[1] J.H.A. Peeters, Patent WO2010008293, Sandwich panel and method for producing such a panel, FiberCore IP bv, 2009-2010.

[2] J.H.A. Peeters, Patent WO2010059048, Method of producing a panel and a core therefor, FiberCore IP bv, 2009-2010.

[3] W. De Corte, A. Jansseune, W. Van Paepegem & J. Peeters, Structural behaviour and robustness assessment of an Infracore Inside bridge deck specimen subjected to static and dynamic local loading, Proceedings of the 21st International Conference on Composite Materials, Xi'an, 20-25th August 2017,pp1-8, 2017.

[4] W. de Corte, A. Jansseune, W. Van Paepegem & J. Peeters., Elastic Properties and Failure Behavior of Tiled Laminate Composites, Key Engineering Materials, vol. 774, pp. 564-569, 2018.

[5] M. Veltkamp & J. Peeters, Hybrid Bridge Structure Composed of Fibre Reinforced Polymers and Steel, Structural Engineering International, 24(3), pp. 425-427, 2014.

[6] Elamx² Composite Calculator, https://tu-dresden.de/ing/maschinenwesen/ilr/lft/elamx2/elamx.

[7] ASTM International Standard test method for short-beam strength of polymer matrix composite materials and their laminates, 2000.